J. Fluid Mech. (2013), *vol.* 717, *pp.* 361–375.
doi:10.1017/jfm.2012.576

Distributed lock-in drives broadband vortex-induced vibrations of a long flexible cylinder in shear flow

Rémi Bourguet[1],†, George Em Karniadakis[2] and Michael S. Triantafyllou[3]

[1]Institut de Mécanique des Fluides de Toulouse, Université de Toulouse and CNRS, Toulouse, 31400, France

[2]Brown University, Providence, RI 02912, USA

[3]Massachusetts Institute of Technology, Cambridge, MA 02139, USA

(Received 4 August 2012; revised 4 August 2012; accepted 17 November 2012; first published online 1 February 2013)

A slender flexible body immersed in sheared cross-flow may exhibit vortex-induced vibrations (VIVs) involving a wide range of excited frequencies and structural wavenumbers. The mechanisms of broadband VIVs of a cylindrical tensioned beam of length-to-diameter aspect ratio 200 placed in shear flow, with an exponentially varying profile along the span, are investigated by means of direct numerical simulation. The Reynolds number is equal to 330 based on the maximum velocity, for comparison with previous work on narrowband vibrations in linear shear flow. The flow is found to excite the structure at a number of different locations under a condition of wake–body synchronization, or lock-in. Broadband responses are associated with a distributed occurrence of the lock-in condition along the span, as opposed to the localized lock-in regions limited to the high inflow velocity zone, reported for narrowband vibrations in sheared current. Despite the instantaneously multi-frequency nature of broadband responses, the lock-in phenomenon remains a locally mono-frequency event, since the vortex formation is generally synchronized with a single vibration frequency at a given location. The spanwise distribution of the excitation zones induces travelling structural waves moving in both directions; this contrasts with the narrowband case where the direction of propagation toward decreasing inflow velocity is preferred. A generalization of the mechanism of phase-locking between the in-line and cross-flow responses is proposed for broadband VIVs under the lock-in condition. A spanwise drift of the in-line/cross-flow phase difference is identified for the high-wavenumber vibration components; this drift is related to the strong travelling wave character of the corresponding structural waves.

Key words: flow-structure interactions, vortex shedding, vortex streets

1. Introduction

Vortex formation downstream of a slender flexible structure with a bluff cross-section induces unsteady forces on the body and can result in structural vibrations.

† Email address for correspondence: bourguet@imft.fr

Vortex-induced vibrations (VIVs) of long deformable bodies are encountered in a number of physical systems, especially in ocean and offshore engineering systems, where they cause increased fatigue damage, and sometimes failure of cables and marine risers. The prediction and attenuation of such vibrations require detailed understanding of the distributed fluid–structure interactions involved in their development.

The significantly simpler problem of a rigid circular cylinder, which is either free to move or forced to oscillate in the cross-flow direction within a uniform current, has served as the canonical problem to study the fundamentals of VIV (Bearman 1984, 2011; Mittal & Tezduyar 1992; Carberry, Sheridan & Rockwell 2001; Williamson & Govardhan 2004; Klamo, Leonard & Roshko 2006; Leontini, Thompson & Hourigan 2006). Maximum-amplitude self-excited oscillations occur when the frequency of vortex formation is relatively close to the natural frequency of the structure; then the frequency of vortex shedding can be entrained to become equal to the frequency of vibration; this condition of wake–body synchronization is referred to as lock-in. Under lock-in, the vortex shedding frequency can be driven far from the Strouhal frequency; also, the vibration frequency can shift considerably away from the original natural frequency in still water due to changes in the value of the effective added mass (Williamson & Govardhan 2004). Substantial changes in the cross-flow response and fluid forces were noted when the rigid cylinder is also allowed to move in the in-line direction (Sarpkaya 1995; Jeon & Gharib 2001; Jauvtis & Williamson 2004; Dahl *et al.* 2007, 2010).

The VIVs of slender flexible cylinders in non-uniform currents have typically high structural wavenumbers and consist of a mixture of standing and travelling wave patterns, often involving multiple frequencies of response (Newman & Karniadakis 1997; Chaplin *et al.* 2005; Lie & Kaasen 2006; Lucor, Mukundan & Triantafyllou 2006; Vandiver, Jaiswal & Jhingran 2009; Bourguet, Karniadakis & Triantafyllou 2011*a*). Since the vortex shedding frequency past a stationary cylinder depends on the inflow velocity, a sheared oncoming current can potentially excite a range of natural frequencies for a long deformable cylindrical structure. The shear rate in the oncoming current and the profile of the flow velocity component normal to the structure are important factors in the transition from mono- to multi-frequency vibrations (Vandiver, Allen & Li 1996; Bourguet, Lucor & Triantafyllou 2012). For a flexible cylinder in linear shear flow two types of responses were found, either a mono-frequency or a narrowband multi-frequency response, exhibiting very similar features (Bourguet *et al.* 2012). For the latter case, a limited range of high-wavenumber vibration components is excited in each direction (in-line and cross-flow). In both types of response, energy is transferred from the fluid to the structure under a locally mono-frequency lock-in condition, which occurs in a spanwise region located in the high-velocity zone and characterized by an in-line/cross-flow response phase difference that lies within a specific range.

Lucor, Imas & Karniadakis (2001) and Lucor *et al.* (2006) showed that exponentially sheared currents can trigger cross-flow vibrations involving a much wider range of frequencies, associated with both low and high spatial wavenumbers. The main characteristics of these broadband structural responses can be captured by means of an empirical representation of the flow through a distribution of wake oscillators (Violette, de Langre & Szydlowski 2010). However, previous studies did not provide information concerning wake patterns, fluid–structure energy transfer or regarding the synchronization of the in-line and cross-flow vibrations.

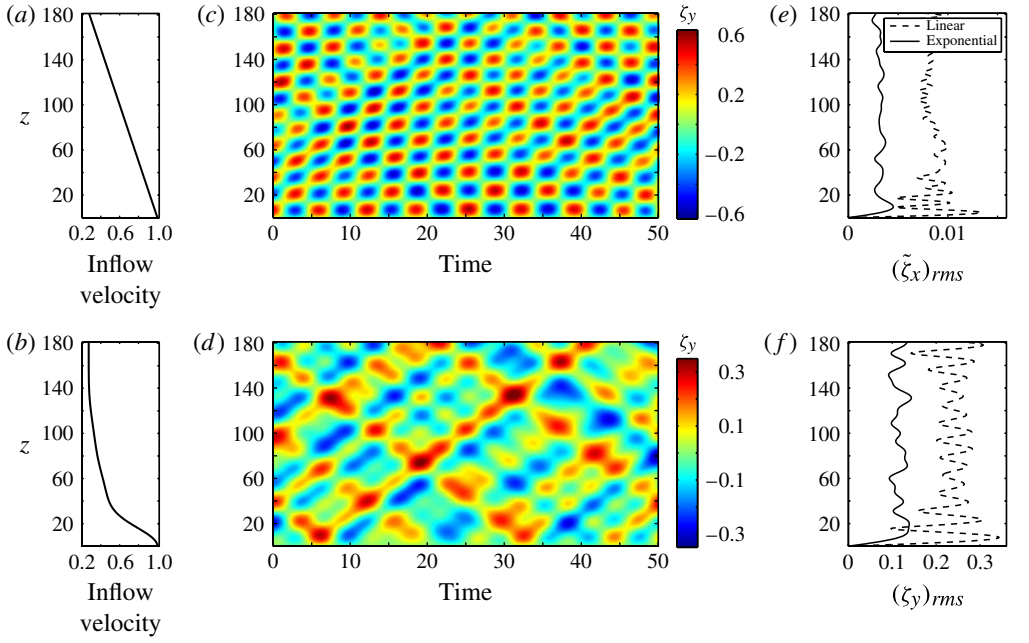

FIGURE 1. (*a*) Linear and (*b*) exponential inflow velocity profiles; (*c,d*) selected time series of the cross-flow displacement along the span in the (*c*) linear and (*d*) exponential shear flow cases; (*e,f*) r.m.s. value of the (*e*) in-line displacement fluctuation and (*f*) cross-flow displacement, along the span.

Hence, the validity of the fluid–structure interaction mechanisms identified in the narrowband VIV case is under question for broadband responses and the possible occurrence of new phenomena needs to be investigated. To address these aspects, a combined wake–body analysis of broadband VIVs is presented on the basis of high-resolution simulation results issued from direct numerical simulation of the flow past a tensioned beam, in conditions similar to those considered in a previous work on narrowband responses reported by Bourguet *et al.* (2011*a*).

2. Formulation and numerical method

Direct numerical simulation of the incompressible Navier–Stokes equations is used to predict the flow past a flexible cylinder exposed to a sheared oncoming cross-flow. The inflow is parallel to the global x-axis and sheared along the global z-axis. The current velocity profile is similar to the exponential profiles employed in the works of Lucor *et al.* (2001, 2006), where structural vibrations involving a wide range of frequencies have been observed. For comparison purposes, some results concerning narrowband VIVs in linear shear flow reported in a previous paper (Bourguet *et al.* 2011*a*) are also presented. The linear and exponential velocity profiles are plotted in figures 1(*a*) and 1(*b*). In both cases, the ratio between the maximum and the minimum inflow velocities is set equal to 3.67. The cylinder diameter D and the maximum oncoming flow velocity U, which occurs at $z = 0$, are used to non-dimensionalize the physical variables. The Reynolds number based on D and the inflow velocity varies from 90 to 330, a range where narrowband multi-frequency vibrations have been observed in linear shear flow as reported in the above-mentioned work.

The cylinder has a circular cross-section and an aspect ratio of $L/D = 200$, where L is the length in its equilibrium position. It is pinned at both ends and free to move in the in-line (x) and cross-flow (y) directions. The structural/fluid mass ratio is defined as $m = \rho_c/\rho_f D^2$, where ρ_c is the cylinder mass per unit length and ρ_f the fluid density (Newman & Karniadakis 1997). The tension, bending stiffness and damping of the structure are designated by T, EI and K, respectively. The in-line and cross-flow displacements of the cylinder are denoted by ζ_x and ζ_y and the in-line and cross-flow fluid force coefficients by C_x and C_y. The influence of gravity is neglected. The cylinder structural dynamics are governed by an extensible tensioned beam model, expressed as follows in non-dimensional formulation:

$$\frac{\partial^2 \zeta_{\{x,y\}}}{\partial t^2} - \omega_c^2 \frac{\partial^2 \zeta_{\{x,y\}}}{\partial z^2} + \omega_b^2 \frac{\partial^4 \zeta_{\{x,y\}}}{\partial z^4} + \frac{K}{m} \frac{\partial \zeta_{\{x,y\}}}{\partial t} = \frac{C_{\{x,y\}}}{2m}. \tag{2.1}$$

Here t denotes the non-dimensional time variable, and ω_c and ω_b denote the cable and beam phase velocities, defined as $\omega_c^2 = T/m$ and $\omega_b^2 = EI/m$, respectively. As in previous simulations concerning linear shear flow, the mass ratio is equal to six ($m = 6$) and the structural damping is set to zero ($K = 0$) to allow maximum-amplitude oscillations. The cable and beam phase velocities are set to comparable values, $(\omega_c, \omega_b) = (5, 10)$ in the present exponential shear case versus $(\omega_c, \omega_b) = (4.55, 9.09)$ in the linear shear case (Bourguet *et al.* 2011*a*).

The coupled fluid–structure system is solved by the parallelized code Nektar, based on the spectral/*hp* element method (Karniadakis & Sherwin 1999). Details concerning validation of the numerical method have been reported by Newman & Karniadakis (1997) and Evangelinos & Karniadakis (1999). The computational domain ($50D$ downstream and $20D$ in front, above and below the cylinder) and discretization (2175 elements with polynomial order $p = 7$ in the (x, y) planes and 512 complex Fourier modes in the z direction) are the same as in Bourguet *et al.* (2011*a*). A buffer region (not presented in the following) is used to enforce the spanwise periodicity of the inflow velocity profile implied by the Fourier expansion used in the z direction; this technique has been validated in the above-mentioned reference. The present analysis is based on time series of more than 300 time units, collected after convergence of the time-averaged in-line displacement of the body.

3. Broadband structural responses

The mixed standing–travelling wave nature of the structural vibrations is illustrated in figure 1(*c*,*d*), where selected time series of the cross-flow displacement are plotted along the span for the linear and exponential flow velocity profiles. In the case of linear shear, the structural waves appear mainly oriented from the high to the low inflow velocity regions. In contrast, no preferential orientation of the waves can be identified in the exponential shear case. Root mean square (r.m.s.) values of the vibration amplitudes along the span are presented in figure 1(*e*,*f*). The amplitudes reached in the cross-flow direction and the amplitude ratio of approximately two between the linear and exponential shear cases are comparable with those reported for flexible cylinders allowed to move in the cross-flow direction only within similar currents (Lucor *et al.* 2006). The ratio between the maximum r.m.s. values of the cross-flow and in-line response amplitudes is similar for both profiles; the impact of the Reynolds number on this ratio, which decreases at higher Reynolds number, has been reported in a previous work (Bourguet *et al.* 2011*a*).

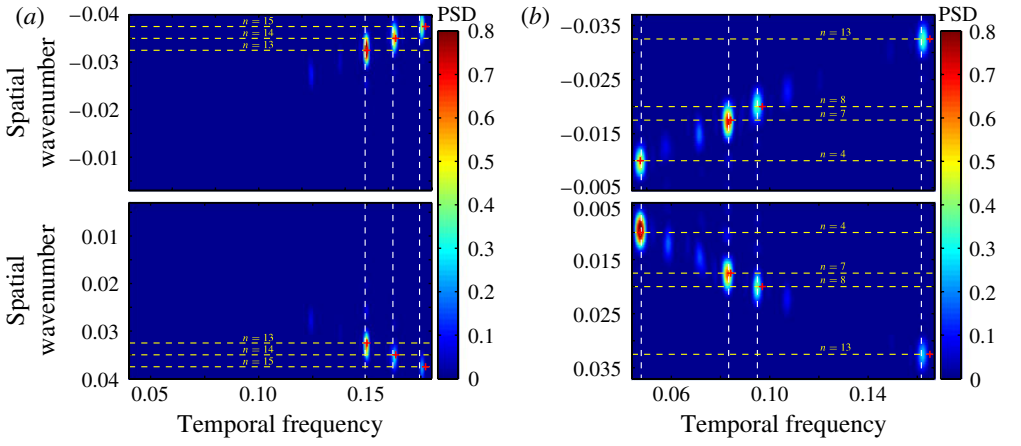

FIGURE 2. Spatiotemporal spectral analysis of the cross-flow displacement in the (*a*) linear and (*b*) exponential shear flow cases. Selected vibration frequencies are identified by white vertical dashed lines. The wavenumbers of selected sine Fourier modes are indicated by yellow horizontal dashed lines. Red crosses denote the natural frequencies associated with these wavenumbers.

For a better quantification of the cylinder vibrations, a spatiotemporal spectral analysis based on a two-dimensional fast Fourier transform of the structural responses is performed. In figure 2, the cross-flow displacement power spectral density (PSD) is plotted as a function of the temporal frequency and spatial wavenumber, in the linear and exponential shear flow cases. Positive frequencies are considered and thus negative wavenumbers correspond to waves travelling from high- to low-velocity regions (increasing z) while positive wavenumbers are associated with waves travelling in the other direction.

Both inflow velocity profiles lead to multi-frequency vibrations. As reported previously (Bourguet *et al.* 2012), in linear shear flow, the structural response involves a narrow range of excited frequencies. In contrast, the present exponential shear profile leads to a large vibration bandwidth, also observed by Lucor *et al.* (2006) for free oscillations in the cross-flow direction only. The ratio between the maximum and minimum vibration frequencies is equal to 3.4 approximately in the exponential shear case while it is smaller than 1.2 in the linear shear case.

The large frequency bandwidth of the structural response in the exponential shear case is accompanied by the excitation of a wide range of spatial wavenumbers. Each excited frequency is generally associated with a single structural wavenumber. The excited wavenumbers involved in the cross-flow vibration correspond to sine Fourier modes in the range $n \in \{4, 7, 8, 13\}$ with the nth mode defined by $\sin(\pi n z D/L)$. With similar structural parameters, only high wavenumbers associated with three adjacent Fourier modes ($n \in \{13, 14, 15\}$) are noted in the linear shear case. The vibration in the exponential shear case, characterized by a large frequency bandwidth and excitation of both high and low structural wavenumbers, is referred to as a broadband response by comparison with the narrowband response identified previously in linear shear flow.

As also noted in previous studies, each excited frequency in the cross-flow direction can be related, with a ratio of two, to an excited frequency in the in-line direction. As a consequence, the in-line structural response also presents a clear

narrowband or broadband character, depending on the oncoming flow velocity profile. In contrast to the pairs of in-line/cross-flow response frequencies, the corresponding excited wavenumbers generally exhibit a ratio different from two; this behaviour is expected because of the nonlinear frequency–wavenumber dispersion relation of tensioned beams. The following dispersion relation may be used to estimate the natural frequency f associated with the structural wavenumber k:

$$f = \sqrt{\frac{m}{m + \frac{\pi}{4} C_m}} k \sqrt{\omega_c^2 + 4\pi^2 \omega_b^2 k^2}, \tag{3.1}$$

where C_m is the added mass coefficient induced by the fluid forces in phase with the body acceleration. Selected response frequencies and wavenumbers of selected sine Fourier modes are indicated by dashed lines in figure 2. The natural frequencies corresponding to the identified wavenumbers are indicated by red crosses. These frequencies, based on the above dispersion relation with the fluid added mass coefficient $C_m = 1$, may present significant departures from the actual peaks which can be related to the effective added mass variability.

The comparison of the magnitudes of the negative- and positive-wavenumber PSD peaks at each vibration frequency confirm the occurrence of waves travelling in both directions in the broadband response case, as shown in figure 1(*d*); this aspect will be clarified by the spanwise distribution of the excitation/damping regions in § 5.

In the case of narrowband vibrations, previous work has shown that the structural responses remain instantaneously mono-frequency at a given spanwise location; the overall multi-frequency character is due to a temporal drift of the instantaneous response frequency, which switches among possible response frequencies (Bourguet *et al.* 2011*a*). This behaviour is illustrated in figure 3(*a*) where a time series of the cross-flow displacement in the linear shear case and the corresponding scalogram, i.e. the squared magnitude of the signal's continuous wavelet transform as a function of the frequency and time, are presented.

Herein the question of the instantaneous mono- or multi-frequency nature of broadband vibrations is addressed by a similar time/frequency analysis. A typical time series of the broadband cross-flow response in a spanwise region where the four vibration frequencies exhibit significant contributions is plotted in figure 3(*b*). In the associated scalogram, a temporal shift similar to the narrowband response behaviour can be noted between two intermediate frequencies (0.083 and 0.095). However, if all four possible vibration frequencies are considered, it is clearly shown that multiple frequencies, and thus multiple structural wavenumbers, can respond simultaneously. As a consequence, the observed broadband VIVs can be regarded as an instantaneously multi-frequency phenomenon.

Next, the occurrence of broadband structural vibrations is related to the fluid–structure interaction mechanisms.

4. Distributed lock-in in shear flow

For a slender flexible body subject to multi-frequency VIVs in non-uniform current, the lock-in condition can be defined at each spanwise location and each cross-flow vibration frequency as the local synchronization between the body oscillation and the vortex formation. The condition is referred to as non-lock-in if the structural vibration and the vortex shedding frequencies do not coincide. The spanwise region which envelopes all the locally locked-in locations at a given vibration frequency is

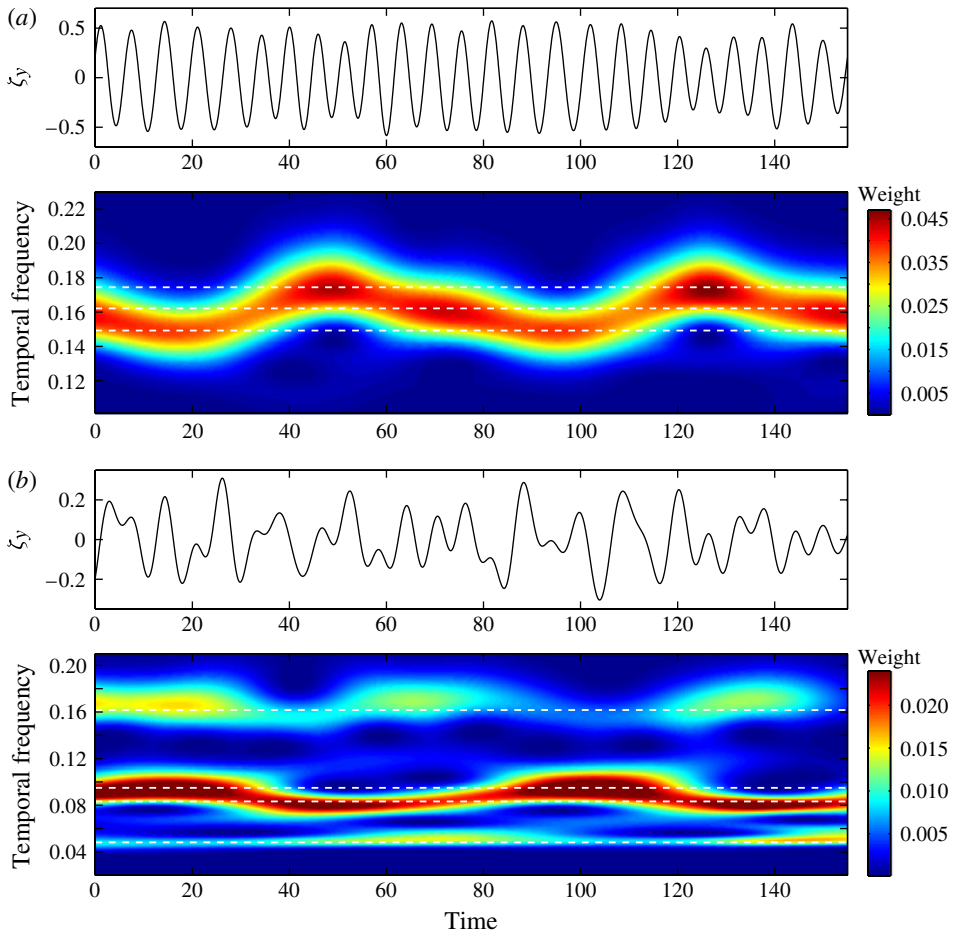

FIGURE 3. Selected time series of the cross-flow displacement and corresponding frequency content as a function of time (scalogram), in the (*a*) narrowband (linear shear flow, $z = 7.5$) and (*b*) broadband (exponential shear flow, $z = 9.4$) response cases. Dashed lines denote the vibration frequencies identified in figure 2.

referred to as the lock-in region. The vortex shedding frequency is established by means of the PSD of the cross-flow component of the flow velocity downstream of the cylinder, which is plotted along the span in the linear and exponential shear flow cases in figure 4(*a*,*b*), respectively. The predominant cross-flow vibration frequencies are indicated by vertical dashed lines in these figures.

Previous studies concerning flexible cylinders subject to mono-frequency or narrowband VIVs in linear shear flow have highlighted a clear spanwise pattern of wake–body synchronization (Lucor *et al.* 2001; Bourguet *et al.* 2011*a*). In this case, as can be observed in figure 4(*a*), an area including all the lock-in regions at the different vibration frequencies can be identified in the high inflow velocity zone. This area covers approximately 35 % of the cylinder length while the rest of the span corresponds to an area of non-lock-in. The question that arises is what lock-in/non-lock-in pattern is associated with broadband VIVs.

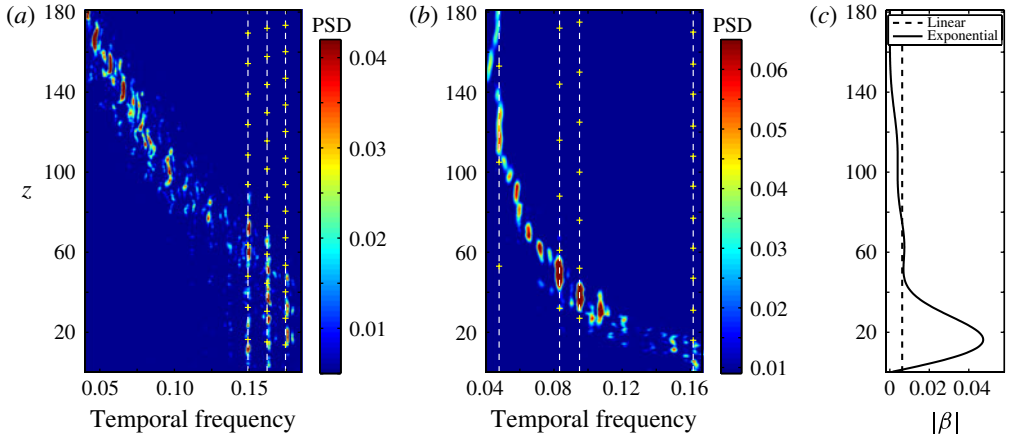

FIGURE 4. (*a,b*) PSD of the cross-flow component of flow velocity along a spanwise line in the wake, in the (*a*) narrowband (linear shear flow, $(x, y) = (20, 0)$) and (*b*) broadband (exponential shear flow, $(x, y) = (15, 0)$) response cases. Dashed lines indicate the frequencies of the cross-flow vibrations identified in figure 2 and yellow crosses show the local minima of the cross-flow vibration PSD, at each frequency. (*c*) Spanwise evolution of the magnitude of the inflow velocity profile shear rate.

In contrast to the case of narrowband vibrations, where the locally locked-in locations are all localized in the high-velocity zone, the broadband response case exhibits a *distributed* occurrence of the lock-in condition along the span, both in the high- and low-velocity zones, as shown in figure 4(*b*).

The ratio between the maximum and minimum inflow velocities and the structural properties in the broadband response case are similar to those considered in the narrowband response case; the change from localized to distributed lock-in is thus triggered by the shear profile. It can be noted that, at each vibration frequency, the lock-in condition may be limited to a spanwise cell bounded by two successive local minima of the cross-flow vibration PSD (equivalent to 'nodes'; shown as yellow crosses in figures 4*a,b*), as for instance for the three highest frequencies in the exponential shear case, but can also occur over several cells. The magnitude of the local shear rate defined as $\beta = (1/U_a)\partial U_l/\partial z$, where U_l and U_a are the local and span-averaged inflow velocities, is plotted along the span in figure 4(*c*), for both velocity profiles. In the case of non-uniform shear rate (figure 4*b*), it appears that no well-defined wake–body synchronization area can be identified in the zone of large shear magnitude ($z \approx 20$), while a wide region of lock-in can be noted in the weakly sheared zone ($z > 110$). This emphasizes the importance of the local shear rate for the occurrence of the lock-in condition; this aspect is currently under investigation. It is recalled that the present work aims at examining the possible extension of the fluid–structure interaction mechanisms, previously studied for narrowband VIVs, to the case of broadband vibrations; and at identifying novel phenomena associated with the modification of the nature of the body response.

In both shear flow cases, the wake is composed of spanwise cells of constant shedding frequency, as also reported for stationary cylinders with varying spanwise conditions (e.g. Gaster 1971; Griffin 1985). The global decrease of the vortex shedding frequency along the span is driven by the decrease of the inflow velocity through the Strouhal relation. Under the lock-in condition, the wake is generally synchronized

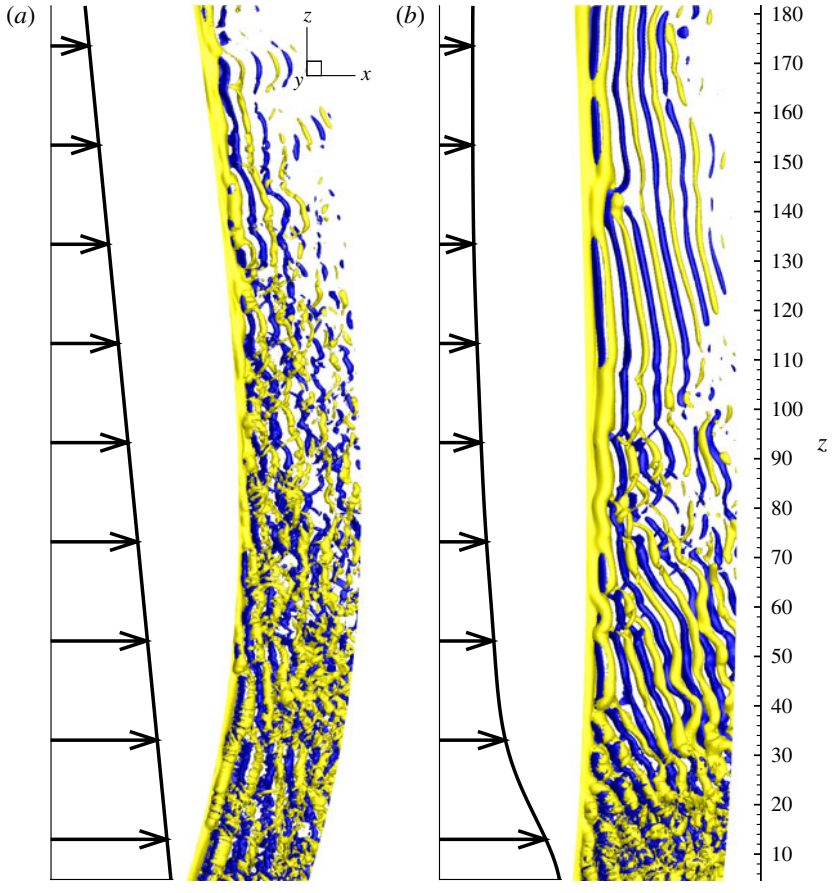

FIGURE 5. (Colour online) Instantaneous isosurfaces of spanwise vorticity downstream of the cylinder: (*a*) narrowband (linear shear flow, $\omega_z = \pm 0.3$) response case; and (*b*) broadband (exponential shear flow, $\omega_z = \pm 0.15$) response case. Part of the computational domain is plotted. Arrows represent the sheared oncoming flow.

with a single structural frequency at each point of the span, even if several vibration frequencies coexist. As a consequence, the lock-in phenomenon remains a locally mono-frequency event, even in the case of broadband responses.

An overview of the wake patterns is presented in figure 5 by means of instantaneous isosurfaces of the spanwise vorticity (z component), for both inflow velocity profiles. The cellular pattern of vortex shedding frequency induces two predominant features in the vortical wake, which are similar for the narrowband and broadband response cases and also comparable with those described for stationary cylinders in shear flow: the spanwise variation of the oncoming flow velocity in each cell of constant vortex shedding frequency leads to an oblique orientation of the vortex rows as they form, while vortex splitting events ensure the continuity of the vortex filaments between two adjacent cells.

Previous experimental and numerical works concerning mono-frequency and narrowband multi-frequency VIV of long flexible cylinders in shear flow have shown that the lock-in condition is generally established through a particular type of figure-of-

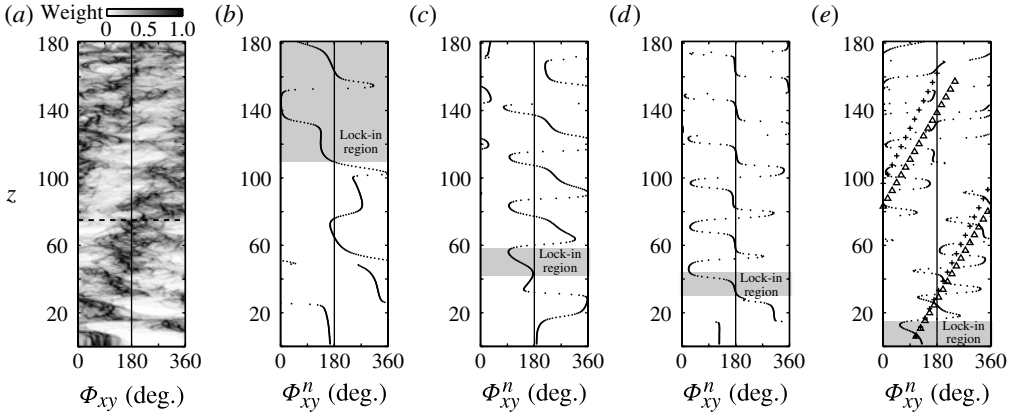

FIGURE 6. Phase difference between the in-line and cross-flow displacements, along the cylinder span: (*a*) histogram issued from the total displacement signals in the narrowband response case (Φ_{xy} defined in (4.1)) and (*b–e*) difference between the spatial phases of the principal components of the displacements presenting a frequency ratio of 2 in the broadband response case (Φ^n_{xy} defined in (4.3)); (*b*) $f^n = 0.048$; (*c*) $f^n = 0.083$; (*d*) $f^n = 0.095$; (*e*) $f^n = 0.162$. In (*a*), the limit of the spanwise zone including all the lock-in regions (global lock-in region) is denoted by a horizontal dashed line. In (*b–e*), the lock-in region associated with each vibration frequency is coloured in grey. In (*e*), the phase differences in the case of pure travelling waves, based on the effective excited wavenumbers and the excited wavenumbers estimated through the dispersion relation, are indicated by triangles and crosses, respectively.

eight trajectories, the counter-clockwise orbits, where the body moves upstream at the extrema of the cross-flow oscillation (Vandiver *et al.* 2009; Bourguet *et al.* 2011*a*,*b*). Dahl *et al.* (2007) reported that the shed vorticity is stronger due to the upstream motion of the cylinder and that the closer proximity of the body and the recently shed vortices induced by these trajectories leads to a specific phasing between cylinder motion and vortex suction forces, resulting in stable vibrations.

The phenomenon of phase-locking between the in-line and cross-flow responses under the condition of wake–body synchronization is illustrated in figure 6(*a*) where the histogram of phase difference between the narrowband vibrations occurring in each direction is plotted along the span. The phase difference is defined as

$$\Phi_{xy} = \left[p\phi_x - q\phi_y, \text{mod } 360^\circ\right], \tag{4.1}$$

where ϕ_x and ϕ_y are the instantaneous phases of the in-line and cross-flow responses. The pair $(p, q) = (1, 2)$ is chosen here since the synchronization is studied for a frequency ratio of two between the responses in each direction. In this figure, a horizontal dashed line indicates the limit of the area including all the locked-in locations; this area is referred to as the global lock-in region. As previously mentioned, Φ_{xy} lies mainly in the range associated with counter-clockwise trajectories ($\Phi_{xy} \in [0^\circ, 180^\circ]$) in this region.

The existence of a similar phase-locking mechanism of the responses for broadband VIV is investigated in the following. In this case, multiple frequencies can respond simultaneously at each spanwise location. The in-line and cross-flow displacements

can be approximated using $N+1$ temporal Fourier modes:

$$\zeta_{\{x,y\}}(z,t) \approx \sum_{n=-N/2}^{N/2} a^n_{\{x,y\}}(z)\exp(2\pi \mathrm{i} f^n t)$$
$$= \sum_{n=-N/2}^{N/2} |a^n_{\{x,y\}}|(z)\exp\left(\mathrm{i}\left(2\pi f^n t + \psi^n_{\{x,y\}}(z)\right)\right) \tag{4.2}$$

where $f^n = n/T_s$ and T_s is the sampling period. The complex modal coefficients a^n_x and a^n_y are written in terms of their moduli and their spatial phases ψ^n_x and ψ^n_y. The phase difference between the in-line and cross-flow responses occurring at frequencies $2f^n$ and f^n, respectively, is evaluated as follows:

$$\Phi^n_{xy} = [\psi^{2n}_x - 2\psi^n_y, \mathrm{mod}\ 360^\circ]. \tag{4.3}$$

The spanwise evolutions of the phase differences associated with the four predominant cross-flow vibration frequencies are plotted in figure 6(*b–e*). In each plot, the lock-in region including the locations locally locked-in at the studied frequency is indicated in grey. Within each lock-in region, the phase difference remains smaller than 180°. It can be noted that the zone where $\Phi^n_{xy} > 180^\circ$, for $z \approx 155$ at $f = 0.048$, is associated with a local interruption of the lock-in condition in figure 4(*b*). Hence, the components of the in-line and cross-flow vibrations that are locally involved in the lock-in phenomenon remain in a specific phase-difference range. Therefore, the mechanism of vibration phase locking under the lock-in condition can be generalized to the case of broadband VIV.

Another feature can be identified in the in-line/cross-flow response synchronization: the vibration components involving high structural wavenumbers exhibit a clear drift of their phase difference along the span, as can be observed in figure 6(*e*). This phenomenon also occurs in the mono-frequency and narrowband multi-frequency VIV cases (Bourguet *et al.* 2011*a*,*b*); it is related to the pronounced travelling wave character of the response components, as discussed in § 5.

In the next section, the fluid–structure energy transfer is studied in light of the distributed occurrence of the lock-in phenomenon and the impact of the spanwise pattern of energy transfer on the resulting vibrations is analysed.

5. Fluid–structure energy transfer

The transfer of energy between the flow and the oscillating structure is quantified by means of the time-averaged fluid force coefficient in phase with the cylinder velocity. In the cross-flow direction, it can be defined as

$$C_{fv} = \frac{\sqrt{2}\left\langle C_y \dfrac{\partial \zeta_y}{\partial t}\right\rangle}{\sqrt{\left\langle \left(\dfrac{\partial \zeta_y}{\partial t}\right)^2\right\rangle}}, \tag{5.1}$$

where $\langle\cdot\rangle$ denotes the time-averaging operator. The spanwise evolution of C_{fv} in the narrowband response case is plotted in figure 7(*a*) (lower axis, full line). The area encompassing the lock-in regions at all vibration frequencies, the global lock-in region, is indicated in grey in this figure. As also reported in previous work

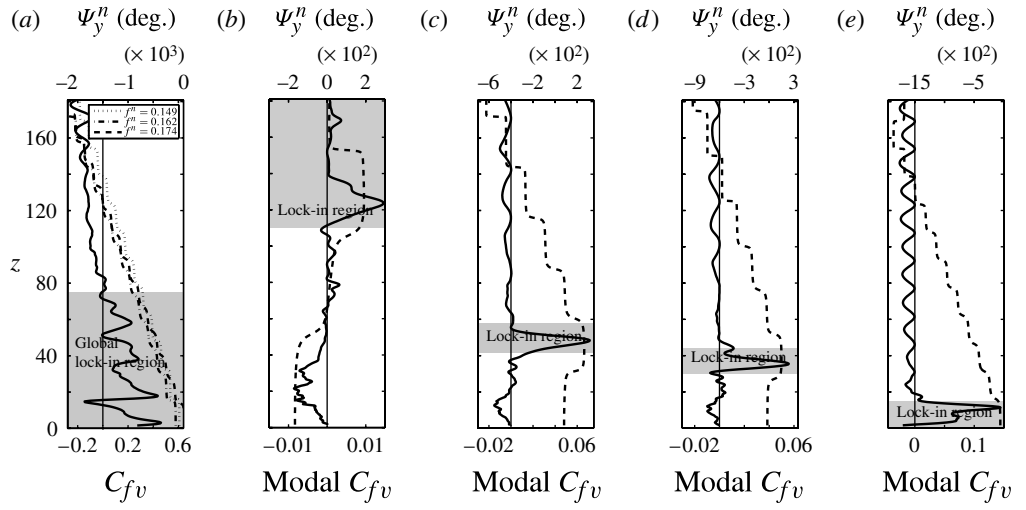

FIGURE 7. Time-averaged cross-flow force coefficient in phase with the cylinder velocity (lower axis, full line) and spatial phase of the cross-flow vibration (upper axis, dashed line), along the cylinder span: (*a*) C_{fv} and spatial phases of the three predominant vibration components in the narrowband response case; (*b–e*) modal C_{fv} and spatial phase of the vibration component at frequency; (*b*) $f^n = 0.048$; (*c*) $f^n = 0.083$; (*d*) $f^n = 0.095$; and (*e*) $f^n = 0.162$, in the broadband response case. The global lock-in region (in *a*) and the lock-in region associated with each vibration frequency (in *b–e*) are coloured in grey.

(Bourguet *et al.* 2011*a*), the zone of positive energy transfer, i.e. where the flow excites the structural vibrations ($C_{fv} > 0$), is located within the global lock-in region. Outside of this region, the flow damps the body oscillations ($C_{fv} < 0$).

In the broadband response case, a frequency decomposition of C_{fv} is employed to monitor the spanwise evolution of the energy transfer at the vibration frequencies, as shown in figure 7(*b–e*) (lower axis, full line). Body excitation by the flow occurs within the lock-in regions (areas in grey). However, unlike the narrowband case, the excitation zones are distributed along the length of the cylinder, high-wavenumber vibrations being excited on the high oncoming flow velocity side and low-wavenumber responses on the low inflow velocity side.

The above analysis raises the question of the impact of the spanwise distribution of the excitation/damping regions on the orientation of the structure travelling wave responses. To address this question, the spatial phases ψ_y^n of the waves associated with the predominant vibration frequencies are plotted along the span in figure 7 (upper axis, dashed lines). Positive frequencies are considered ($n \in [0, N/2]$); the waves are thus travelling in the direction of decreasing ψ_y^n. Pure travelling waves would exhibit linear evolutions. The sawtooth perturbations are due to the underlying standing wave character of the responses. For each excited frequency and regardless the narrowband or broadband nature of the response, the structural wave travels from the excitation region toward zones of damping by the flow. This observation is also verified for the in-line vibrations, even though C_{fv} presents noisier patterns. As a consequence, the overall broadband structural response is composed of waves travelling in both directions, i.e. decreasing and increasing inflow velocity directions. This behaviour contrasts with the narrowband response case where the travelling waves are all oriented from the high to the low inflow velocity regions.

The well-defined travelling wave character of the high-wavenumber vibration components, which is induced by the distribution of the excitation and damping areas, causes a persistent spanwise drift of the in-line/cross-flow phase difference. In the case of a pure travelling wave, the phase of the nth mode is $2\pi f^n t + 2\pi k^n_{\{x,y\}} z + \eta^n_{\{x,y\}}$, where $k^n_{\{x,y\}}$ is the excited structural wavenumber and $\eta^n_{\{x,y\}}$ a constant phase lag. The unwrapped phase difference between pairs of in-line/cross-flow vibration components becomes

$$\Phi^n_{xy} = 2\pi \left(k^{2n}_x - 2k^n_y\right) z + \eta^{2n}_x - 2\eta^n_y. \tag{5.2}$$

As a result, the spanwise evolution of Φ^n_{xy} depends linearly on the difference between the in-line wavenumber and a value equal to twice the cross-flow wavenumber. The actual behaviour of the phase difference, in the present case of mixed standing–travelling wave vibrations, follows closely the trend of pure travelling wave responses, involving the effective excited wavenumbers (triangles in figure 6*e*). The zig-zagging modulations are induced by the underlying standing wave patterns; pure standing waves would lead to a discontinuous evolution of Φ^n_{xy} with two synchronized states separated by 180° phase jumps located at the nodes of the in-line response. The phase difference (5.2), based on estimates of the excited wavenumbers through the dispersion relation (3.1) with $C_m = 1$ and the effective response frequencies, differs slightly from the actual behaviour (crosses in figure 6*e*). This illustrates the effect of the previously mentioned deviation from the dispersion relation, which assumes the added mass coefficient is constant. No well-defined phase difference drift is noted for the vibration components involving lower spatial wavenumbers due their stronger standing wave nature.

6. Conclusions

The broadband VIVs of a long cylindrical tensioned beam in sheared current have been investigated by means of direct numerical simulation. Mixed standing–travelling wave vibrations including a wide range of excited frequencies and structural wavenumbers have been triggered by an exponentially sheared inflow velocity profile, with a maximum Reynolds number equal to 330.

For narrowband responses in linear shear flow, the lock-in condition is localized and appears over a limited portion of the span, located in the high-velocity zone. In contrast, for broadband VIVs involving similar structure and maximum/minimum inflow velocity ratio, we find that the lock-in condition is distributed and may occur along the entire cylinder length, and hence can occur in high- and low-velocity regions. For each vibration frequency, the flow excites the structure oscillations under the lock-in condition and damps them in the non-lock-in zones. The structural waves move from the excitation to the damping regions; due to the distribution of the excitation zones along the span, waves travelling in both directions can be noted; unlike the narrowband case where the direction of decreasing inflow velocity is always preferred.

At a given spanwise location, we find that several frequencies and structural wavenumbers can respond simultaneously, leading to instantaneously multi-frequency vibrations; such vibrations differ from the instantaneously mono-frequency responses noted for narrowband VIVs. However, the lock-in phenomenon remains a locally mono-frequency event since the vortex shedding is generally synchronized with a single vibration frequency at each point of the span. The wake pattern, composed of spanwise cells of constant vortex shedding frequency, is characterized by oblique

vortex shedding and vortex splittings, as also observed for a long cylinder, subject to narrowband VIVs or stationary, in shear flow.

The phase difference between the components of the broadband in-line and cross-flow vibrations occurring with a frequency ratio of two and locally involved in the lock-in phenomenon, remains within a particular range, associated with counter-clockwise figure-of-eight orbits in the case of mono-frequency responses. As a result, we find that the mechanism of phase locking under the lock-in condition, previously identified for mono-frequency and narrowband responses, also applies to the studied broadband VIV. In addition, we find that a regular spanwise drift of the in-line/cross-flow phase difference, similar to the drift observed for mono-frequency and narrowband VIV, appears for the high-wavenumber vibration components of the broadband responses, due to their pronounced travelling wave character.

Acknowledgements

The authors wish to acknowledge support from the BP-MIT Major Projects Programme, monitored by M. Tognarelli and P. Beynet; and the Office of Naval Research under Grants N00014-07-1-0135 and N00014-07-1-0446, monitored by T. Swean, Jr.

REFERENCES

BEARMAN, P. W. 1984 Vortex shedding from oscillating bluff bodies. *Annu. Rev. Fluid Mech.* **16**, 195–222.

BEARMAN, P. W. 2011 Circular cylinder wakes and vortex-induced vibrations. *J. Fluids Struct.* **27**, 648–658.

BOURGUET, R., KARNIADAKIS, G. E. & TRIANTAFYLLOU, M. S. 2011*a* Vortex-induced vibrations of a long flexible cylinder in shear flow. *J. Fluid Mech.* **677**, 342–382.

BOURGUET, R., LUCOR, D. & TRIANTAFYLLOU, M. S. 2012 Mono- and multi-frequency vortex-induced vibrations of a long tensioned beam in shear flow. *J. Fluids Struct.* **32**, 52–64.

BOURGUET, R., MODARRES-SADEGHI, Y., KARNIADAKIS, G. E. & TRIANTAFYLLOU, M. S. 2011*b* Wake–body resonance of long flexible structures is dominated by counter-clockwise orbits. *Phys. Rev. Lett.* **107**, 134502.

CARBERRY, J., SHERIDAN, J. & ROCKWELL, D. 2001 Forces and wake modes of an oscillating cylinder. *J. Fluids Struct.* **15**, 523–532.

CHAPLIN, J. R., BEARMAN, P. W., HUERA-HUARTE, F. J. & PATTENDEN, R. J. 2005 Laboratory measurements of vortex-induced vibrations of a vertical tension riser in a stepped current. *J. Fluids Struct.* **21**, 3–24.

DAHL, J. M., HOVER, F. S., TRIANTAFYLLOU, M. S., DONG, S. & KARNIADAKIS, G. E. 2007 Resonant vibrations of bluff bodies cause multivortex shedding and high frequency forces. *Phys. Rev. Lett.* **99**, 144503.

DAHL, J. M., HOVER, F. S., TRIANTAFYLLOU, M. S. & OAKLEY, O. H. 2010 Dual resonance in vortex-induced vibrations at subcritical and supercritical Reynolds numbers. *J. Fluid Mech.* **643**, 395–424.

EVANGELINOS, C. & KARNIADAKIS, G. E. 1999 Dynamics and flow structures in the turbulent wake of rigid and flexible cylinders subject to vortex-induced vibrations. *J. Fluid Mech.* **400**, 91–124.

GASTER, M. 1971 Vortex shedding from circular cylinders at low Reynolds numbers. *J. Fluid Mech.* **46**, 749–756.

GRIFFIN, O. M. 1985 Vortex shedding from bluff bodies in a shear flow: a review. *Trans. ASME J. Fluids Engng* **107**, 298–306.

JAUVTIS, N. & WILLIAMSON, C. H. K. 2004 The effect of two degrees of freedom on vortex-induced vibration at low mass and damping. *J. Fluid Mech.* **509**, 23–62.

JEON, D. & GHARIB, M. 2001 On circular cylinders undergoing two-degree-of-freedom forced motions. *J. Fluids Struct.* **15**, 533–541.

KARNIADAKIS, G. E. & SHERWIN, S. 1999 *Spectral/HP Element Methods for CFD*, 1st edn. Oxford University Press.

KLAMO, J. T., LEONARD, A. & ROSHKO, A. 2006 The effects of damping on the amplitude and frequency response of a freely vibrating cylinder in cross-flow. *J. Fluids Struct.* **22**, 845–856.

LEONTINI, J. S., THOMPSON, M. C. & HOURIGAN, K. 2006 The beginning of branching behaviour of vortex-induced vibration during two-dimensional flow. *J. Fluids Struct.* **22**, 857–864.

LIE, H. & KAASEN, K. E. 2006 Modal analysis of measurements from a large-scale VIV model test of a riser in linearly sheared flow. *J. Fluids Struct.* **22**, 557–575.

LUCOR, D., IMAS, L. & KARNIADAKIS, G. E. 2001 Vortex dislocations and force distribution of long flexible cylinders subjected to sheared flows. *J. Fluids Struct.* **15**, 641–650.

LUCOR, D., MUKUNDAN, H. & TRIANTAFYLLOU, M. S. 2006 Riser modal identification in CFD and full-scale experiments. *J. Fluids Struct.* **22**, 905–917.

MITTAL, S. & TEZDUYAR, T. E. 1992 A finite element study of incompressible flows past oscillating cylinders and aerofoils. *Intl J. Numer. Meth. Fluids* **15**, 1073–1118.

NEWMAN, D. J. & KARNIADAKIS, G. E. 1997 A direct numerical simulation study of flow past a freely vibrating cable. *J. Fluid Mech.* **344**, 95–136.

SARPKAYA, T. 1995 Hydrodynamic damping, flow-induced oscillations, and biharmonic response. *J. Offshore Mech. Arctic Engng* **117**, 232–238.

VANDIVER, J. K., ALLEN, D. & LI, L. 1996 The occurrence of lock-in under highly sheared conditions. *J. Fluids Struct.* **10**, 555–561.

VANDIVER, J. K., JAISWAL, V. & JHINGRAN, V. 2009 Insights on vortex-induced, travelling waves on long risers. *J. Fluids Struct.* **25**, 641–653.

VIOLETTE, R., DE LANGRE, E. & SZYDLOWSKI, J. 2010 A linear stability approach to vortex-induced vibrations and waves. *J. Fluids Struct.* **26**, 442–466.

WILLIAMSON, C. H. K. & GOVARDHAN, R. 2004 Vortex-induced vibrations. *Annu. Rev. Fluid Mech.* **36**, 413–455.